Physics Letters B 730 (2014) 307–313

Contents lists available at ScienceDirect

Physics Letters B

www.elsevier.com/locate/physletb

Benchmarking nuclear models for Gamow–Teller response

E. Litvinova [a,b,*], B.A. Brown [c,b], D.-L. Fang [b,d], T. Marketin [e], R.G.T. Zegers [c,b,d]

[a] Department of Physics, Western Michigan University, Kalamazoo, MI 49008-5252, USA
[b] National Superconducting Cyclotron Laboratory, Michigan State University, East Lansing, MI 48824-1321, USA
[c] Department of Physics and Astronomy, Michigan State University, East Lansing, MI 48824-1321, USA
[d] Joint Institute for Nuclear Astrophysics, Michigan State University, East Lansing, MI 48824-1321, USA
[e] Physics Department, Faculty of Science, University of Zagreb, Croatia

ARTICLE INFO

Article history:
Received 2 October 2013
Received in revised form 1 February 2014
Accepted 3 February 2014
Available online 6 February 2014
Editor: J.-P. Blaizot

ABSTRACT

A comparative study of the nuclear Gamow–Teller response (GTR) within conceptually different state-of-the-art approaches is presented. Three nuclear microscopic models are considered: (i) the recently developed charge-exchange relativistic time blocking approximation (RTBA) based on the covariant density functional theory, (ii) the shell model (SM) with an extended "jj77" model space and (iii) the non-relativistic quasiparticle random-phase approximation (QRPA) with a Brueckner G-matrix effective interaction. We study the physics cases where two or all three of these models can be applied. The Gamow–Teller response functions are calculated for ^{208}Pb, ^{132}Sn and ^{78}Ni within both RTBA and QRPA. The strengths obtained for ^{208}Pb are compared to data that enable a firm model benchmarking. For the nucleus ^{132}Sn, also SM calculations are performed within the model space truncated at the level of a particle–hole (ph) coupled to vibration configurations. This allows a consistent comparison to the RTBA where ph⊗phonon coupling is responsible for the spreading width and considerable quenching of the GTR. Differences between the models and perspectives of their future developments are discussed.

1. Introduction

In the last decades, nuclear physics has greatly expanded its domain by taking into consideration nuclei away from the valley of stability that are formed as intermediates in astrophysical processes leading to synthesis of heavy elements [1]. However, in spite of many advances made over decades of research, a global high-precision theory for the description of structure properties of these nuclei is still lacking. While nucleosynthesis studies have strongly benefited from the advances in nuclear structure models, astrophysical modeling is still suffering from ambiguities arising from the nuclear physics input. In order to meet the astrophysical needs, theoretical models should be as microscopic and universal as possible. In the context of the astrophysical modeling, it is highly desirable to come to a high-precision solution of the nuclear many-body problem to enable computation of masses, matter and charge distributions, spectra, decay and various reaction rates consistently within the same framework at zero and finite temperatures.

Although lately the three major concepts in low-energy nuclear theory have advanced, namely (i) ab initio approaches, (ii) configuration interaction models (known also as shell-models) and (iii) density functional theories (DFT), they still have to be further developed to satisfy the above-mentioned requirements. Furthermore, each of them has limitations to their applicability [2].

The sectors of the nuclear landscape where the applicability of the different models overlaps are of particular interest because within these sectors the models can be compared and possibly be used to constrain each other. Here we focus on the description of the Gamow–Teller response. Ab initio models can replace the phenomenological input which is traditionally used in the shell model (SM) with the microscopic effective interaction computed from the first principles [3,4]. In turn, the shell model with its very advanced configuration interaction concept can guide the DFT-based developments beyond its standard mean-field and random phase approximations [5,6]. As a feedback, the extended DFT can provide the SM with single-particle input for the systems where experimental information is not available. Thus, in contrast to considering different models as independently developing alternatives, we rather admit their complementarity which can be used for their further advancements.

The spin–isospin response is one of the most important properties of nuclei. The Gamow–Teller (GT) strength distribution, associated with a spin-transfer ΔS of one unit, an isospin transfer ΔT of one unit, and no angular momentum transfer $\Delta L = 0$, provides information for nuclear beta-decay and other weak processes in

* Corresponding author.
E-mail address: elena.litvinova@wmich.edu (E. Litvinova).

http://dx.doi.org/10.1016/j.physletb.2014.02.001

stars. Because GT transitions play an important role in such a wide variety of astrophysical processes, accurate information is required for a large fraction of the nuclear chart. The shell model has been used very successfully to describe the GT response for nuclei in the p, sd and pf shell [7,8]. The major advantage of these calculations is that the configuration interaction (CI) method provides realistic many-body wave functions starting from a realistic nucleon–nucleon interaction that are complete with regard to a valence space consisting of a few orbitals near the Fermi-surface. On the other hand, the major drawback of the SM is that even a modest increase in the size of the valence space used in the calculations results in an exponential growth of the CI dimensions. Nevertheless, recent progress in computer technology, numerical algorithms, and improved nucleon–nucleon effective interactions make it possible to overcome these technical difficulties for certain areas in the chart of nuclei. For example, a recent shell-model analysis was able to take into account all relevant nuclear orbitals necessary for a good description of the GT strength and double beta decay of ^{136}Xe without recourse to artificially small quenching factors [9].

Density functional theory is the only candidate that can provide a description of GTR for the major part of the nuclear chart. However, until recently, the self-consistent DFT-based studies of the GTR were confined only by the quasiparticle random phase approximation (QRPA) [10–13]. Another version of QRPA employs realistic residual interaction of Brueckner G-matrix derived from the CD-Bonn nucleon–nucleon potential [14,15]. This approach has been successfully applied to description of GTR as well as two-neutrino and neutrinoless double beta decay. Recently, large-scale calculations for beta-decay properties of spherical nuclei along the r-process path [16] and neutron-rich deformed nuclei [17] have been reported.

Fragmentation of the GTR has also been extensively addressed, for instance, within the Quasiparticle-Phonon Model [18] and second RPA [19] (see also references therein), however, these developments did not aim at a self-consistent description of GTR and involved adjustable phenomenological effective interactions. An attempt to describe GTR in medium-mass nuclei within a self-consistent particle–phonon coupling model based on various standard Skyrme parameterizations of the density functional has been reported recently [5]. Earlier, the relativistic time blocking approximation (RTBA) with fully self-consistent treatment of particle–phonon coupling based on the covariant DFT (CDFT) has been developed for the charge-exchange channel. However, the first application of the charge-exchange RTBA was performed for the analysis of the spin-dipole strength [6].

In this article, the Gamow–Teller response of doubly-magic nuclei is calculated within the frameworks of RTBA, QRPA and SM. We consider the Gamow–Teller response in the following three doubly-magic nuclei: (i) ^{208}Pb, where recently experimental data have become available up to high excitation energy [20], (ii) neutron rich ^{132}Sn, which is of the special interest because it represents a case where the shell-model calculations for GTR are feasible and have been carried out up to high excitation energies and (iii) ^{78}Ni. ^{78}Ni and ^{132}Sn play an important role in some astrophysical r-process scenarios and influence the r-process abundance distributions for nuclei around N = 50 and N = 82.

2. Microscopic models for spin–isospin response

2.1. Relativistic time blocking approximation

Density functional theory can, in principle, provide a description of the low-energy dynamics for the major part of the nuclear chart except the lightest nuclei. However, the DFT alone does not allow a high-precision description of nuclear properties due to very limited treatment of many-body correlations, which are especially important for exotic systems at extremes of nuclear stability. The delicate interplay of various kinds of correlations is responsible for the binding energy, low-energy spectra, shapes and decay properties of loosely-bound systems. Extended DFT is one of the most promising microscopic theories for providing a consistent input for astrophysical modeling.

Recent extensions of the DFT use the relativistic framework [21,22] and include temporal and spatial non-localities in the nucleonic self-energies. In medium-mass and heavy nuclei, the non-local parts of the nucleonic self-energies modeled in terms of coupling between single-particle and collective degrees of freedom are treated perturbatively by means of the nuclear field theory technique [23]. The covariant density functional theory provides a good first approximation to the static part of the nucleonic self-energy, and a very convenient working basis for the consistent treatment of its time-dependent non-local terms [24–26]. The nuclear response function, derived consistently within this formalism in the relativistic time-blocking approximation, involves an energy-dependent residual interaction which is responsible for the spreading mechanism of nuclear excitations in both neutral [27,28] and charge-exchange [6] channels. No additional adjustable parameters are introduced within this approach and the few parameters (8–10) of the CDFT, adjusted at the initial stage to masses and radii of several characteristic nuclei, remain unchanged. Further development of the CDFT is proceeding in two directions: (i) additions beyond the level of the mean-field and random phase approximations for the description of the ground and excited states, respectively, by inclusion of two-particle two-hole and higher configurations, and (ii) an attempt to provide a microscopic derivation of the density functional [29]. These two directions are not independent: only after the proper inclusion of the correlations a correct comparison to data is possible, that, in turn, gives conclusions about the origin of the underlying functional.

The RTBA calculations for the GTR are performed in the following three steps: (i) a relativistic mean field (RMF) solution is obtained by minimization of the covariant density functional with NL3 parametrization [30], (ii) phonon spectrum and coupling vertices for the phonons with $J^\pi = 2^+, 3^-, 4^+, 5^-, 6^+$ are obtained by the self-consistent relativistic RPA (RRPA) solutions [31] and (iii) the Bethe–Salpeter equation is solved for the proton–neutron response function with $J^\pi = 1^+$:

$$R(\omega) = \tilde{R}^0(\omega) + \tilde{R}^0(\omega) W(\omega) R(\omega), \tag{1}$$

where $\tilde{R}^0(\omega)$ is the propagator of the two uncorrelated quasiparticles in the static mean field and the second integral part contains the in-medium nucleon–nucleon interaction $W(\omega)$. The two-body interaction $W(\omega)$ consists of the following static terms and of the terms depending on the frequency ω:

$$W(\omega) = V_\rho + V_\pi + V_{\delta\pi} + \Phi(\omega) - \Phi(0). \tag{2}$$

V_ρ and V_π are the finite-range ρ-meson and the π-meson exchange interactions, respectively. They are derived from the covariant energy density functional and read [12]:

$$V_\rho(1,2) = g_\rho^2 \vec{\tau}_1 \vec{\tau}_2 \left(\beta\gamma^\mu\right)_1 (\beta\gamma_\mu)_2 D_\rho(\mathbf{r}_1, \mathbf{r}_2),$$
$$V_\pi(1,2) = -\left(\frac{f_\pi}{m_\pi}\right)^2 \vec{\tau}_1 \vec{\tau}_2 (\boldsymbol{\Sigma}_1 \boldsymbol{\nabla}_1)(\boldsymbol{\Sigma}_2 \boldsymbol{\nabla}_2) D_\pi(\mathbf{r}_1, \mathbf{r}_2), \tag{3}$$

where g_ρ and f_π are the coupling strengths, D_ρ and D_π are the meson propagators and $\boldsymbol{\Sigma}$ is the generalized Pauli matrix [12]. The Landau–Migdal term $V_{\delta\pi}$ is the contact part of the nucleon–nucleon interaction responsible for the short-range repulsion:

$$V_{\delta\pi}(1,2) = g'\left(\frac{f_\pi}{m_\pi}\right)^2 \vec{\tau}_1\vec{\tau}_2\boldsymbol{\Sigma}_1\boldsymbol{\Sigma}_2\delta(\mathbf{r}_1-\mathbf{r}_2), \tag{4}$$

where the parameter $g' = 0.6$ is adjusted to reproduce experimental data on the excitation energies of the Gamow–Teller resonance in ^{208}Pb and kept fixed in the calculations for other nuclei, relying on the results obtained in Ref. [12] within the relativistic QRPA. The amplitude $\Phi(\omega)$ describes the coupling of the nucleons to vibrations (phonons) generated by the coherent nucleonic oscillations. In the time blocking approximation it has the following operator form:

$$\Phi(\omega) = \sum_{\mu,\eta} g_\mu^{(\eta)\dagger}\tilde{R}^{0(\eta)}(\omega-\eta\omega_\mu)g_\mu^{(\eta)}, \tag{5}$$

where the index μ numerates vibrational modes (phonons) with frequencies ω_μ and generalized particle–vibration coupling (PVC) amplitude matrices $g_\mu^{(\eta)}$, and the index $\eta = \pm 1$ denotes forward and backward components, in full analogy with the neutral-channel case [27]. The energy-dependent effective interaction of Eq. (5) is responsible for the spreading mechanism caused by the coupling between the ph and ph⊗phonon configurations. The phonon space is truncated by the angular momenta of the phonons at $J^\pi = 6^+$ and by their frequencies at 15 MeV. The ph⊗phonon configurations are included up to 30 MeV of the excitation energy. The truncation is justified by the subtraction of the term $\Phi(0)$ in Eq. (2). This subtraction removes double counting of the PVC effects from the residual interaction, guarantees the stability of the solutions for the response function and provides faster convergence of the renormalized PVC amplitude $\Phi(\omega)-\Phi(0)$ with respect to the phonon angular momenta and frequencies. This technique is discussed in detail in Ref. [32].

The strength function $S^P(\omega)$

$$S^P(E,\Delta) = -\frac{1}{\pi}Im\left\langle P^\dagger R(E+i\Delta)P\right\rangle, \tag{6}$$

gives the spectral distribution of the nuclear response for a particular external field P which is, in the present case, expressed by the Gamow–Teller lowering operator:

$$P = \sum_{i=1}^{A}\tau_-^{(i)}\boldsymbol{\Sigma}_i. \tag{7}$$

A finite value of the imaginary part of the energy variable is usually taken of the order of the experimental energy resolution, to make a consistent comparison to data.

2.2. Quasiparticle random phase approximation based on the realistic N–N interaction

The non-relativistic proton–neutron (pn) Quasiparticle Random Phase Approximation has been adopted for the Gamow–Teller (GT) response [11,33,34], and it gives good predictions for the GTR strength distributions with the fulfillment of the Ikeda sum rule [33]. The idea of implementing a realistic nuclear force in QRPA calculations for both spherical and deformed nuclei has also been proposed [14,15]. In this work, we focus on the spherical nuclei and adopt the spherical version of the QRPA with realistic forces.

The QRPA concept is based on the introduction of the quasiparticle creation operator:

$$\alpha_\tau^\dagger = u_\tau c_\tau^\dagger + v_\tau c_{\tilde{\tau}}, \tag{8}$$

where τ indicates proton or neutron and $c^\dagger$ and c are single particle creation and annihilation operators, respectively. The symbol "tilde" marks the time-reversed states. Using these operators with u_τ and v_τ amplitudes of the nuclear BCS solution, we can construct the pn-excitation phonon operator in the form:

$$Q_m^{JM\dagger} = \sum_{pn}\left(X^J_{m;pn}A^{JM\dagger}_{pn} - Y^J_{m;pn}\tilde{A}^{JM}_{pn}\right), \tag{9}$$

where the two-quasiparticle operators are defined as $A^{JM\dagger}_{pn} = [\alpha_p^\dagger\alpha_n^\dagger]_{JM} = C^{JM}_{j_pm_p;j_n-m_n}\alpha_p^\dagger\alpha_n^\dagger$. The energies, the forward X and backward Y amplitudes are the solutions of the QRPA equations derived by the variation method [35]:

$$\begin{pmatrix} A & B \\ B^* & A^* \end{pmatrix}\begin{pmatrix} X \\ Y \end{pmatrix} = \omega\begin{pmatrix} 1 & 0 \\ 0 & -1 \end{pmatrix}\begin{pmatrix} X \\ Y \end{pmatrix}, \tag{10}$$

where $A_{pn,p'n'} = [A_{pn},[H,A^\dagger_{p'n'}]]$ and $B_{pn,p'n'} = [A^\dagger_{pn},[H,\tilde{A}^\dagger_{p'n'}]]$. The Hamiltonian and the detailed expressions for A and B matrices with realistic interactions are presented in Ref. [14].

From the diagonalization of Eq. (10), we can obtain the eigenvalues ω_m and eigenvectors X_m and Y_m which are the energies and the amplitudes of the QRPA excitations. With the realistic forces, we can determine the energies of the excited states in odd–odd daughter nucleus with respect to its ground state (the one with the lowest eigenvalue), and denote: $E_m = \omega_m - \omega_{g.s.}$, where the index m numerates the solutions of Eq. (10). The matrix element of the GT$^-$ transition can be written as:

$$M_m^{GT^-} = \sum_{pn}\langle p||\tau_-\boldsymbol{\sigma}||n\rangle\left(u_pv_nX^{1^+}_{m;pn} - v_pu_nY^{1^+}_{m;pn}\right), \tag{11}$$

and the GT strength function is expressed as follows:

$$S^{GT^-}(E) = \sum_m \delta(E-E_m)\left|M_m^{GT^-}\right|^2. \tag{12}$$

For the QRPA A-matrices of Eq. (10), we use the single particle energies (spe) obtained from the SkX mean field [36]. The realistic interaction in the form of G-matrix elements is obtained from the CD-Bonn potential [37] and adopted here in both particle–hole (ph) and particle–particle (pp) channels as the residual interaction for the QRPA. No proton–neutron pp-interaction is included in the calculations because closed shell nuclei with relatively large asymmetry between the neutron and proton numbers will be considered. In general, the neutron–neutron and proton–proton pairing strength is adjusted to reproduce the observed pairing gaps by the five-point formula [38]. Thus, for the residual interaction we have two adjusted parameters for the particle–hole and particle–particle channels g_{ph} and g_{pp}. The parameter g_{ph} is fitted to reproduce the GTR centroid and we adopt $g_{ph} = 1$ if the experimental data is not available. The constant g_{pp} is fixed equal to 0.6 to avoid collapse of the solution of the QRPA equation. The GTR centroid is not sensitive to g_{pp}.

In this work we consider doubly-magic nuclei, for which the BCS solutions show that there is a sharp change of occupation probabilities around the Fermi surface and that QRPA calculations are mainly reduced to RPA calculations. In the RPA limit the importance of g_{pp} is, in turn, reduced. However, the strength of the pairing interaction is kept finite to retain the calculation scheme established for nearly the entire chart of nuclides.

2.3. Shell model (SM)

One of goals of the large-basis nuclear shell model approach is to use a complete basis within a limited set of single-particle states near the Fermi surface. This method is used extensively in light nuclei such as in the sd-shell (A = 16–40) pf-shell (A = 40 = 80) mass

regions [7]. All of orbitals required to obtain the Ikeda sum-rule for Gamow–Teller strength are contained in the model space. One of the observations for these model spaces is that the experimental B(GT) values extracted from beta decay and charge-exchange reactions are about a factor of two smaller than those calculated. Thus, for the *sd* or *pf* model spaces one needs a reduction (quenching) factor for the Gamow–Teller operator of 0.74–0.77 [39,40]. This quenching is consistent with theoretical calculations of the operator renormalization obtained in second-order perturbation theory [41,42].

For heavier nuclei the number of basis states even for a modest number of orbitals grows exponentially as the number of valence nucleons increases. Thus, the shell model applications are restricted to semi-magic nuclei or those near double-magic nuclei such as ^{132}Sn or ^{208}Pb. Often the orbitals used in the model space are not sufficient to accommodate the Ikeda sum rule. For example, in the region north-west of ^{132}Sn the "jj55" model space if often used. The notation jj55 represents the five orbitals $0g_{7/2}$, $1d_{5/2}$, $1d_{3/2}$, $1s_{1/2}$, $0h_{11/2}$ in between the magic numbers 50 and 82 for protons and neutrons. The $0g_{9/2}$ and $0h_{9/2}$ orbitals need to be added to satisfy the Ikeda sum rule.

One of the applications of these calculations is for the double beta decay of ^{136}Xe. Up until recently the jj55 model space has been used with the understanding that some renormalization of the operators may be related to the restricted model space. For the Gamow–Teller operator that enters into the two-neutrino double beta decay the renormalization might be fixed by reproducing some single and double beta decay rates. In [43] a quenching factor of 0.45 was used to obtain the observed two-neutrino rate. The question is then to what extent other operators such as those for neutrino-less double beta decay are renormalized.

Recently the jj55 model space was enlarged to jj77 where the configurations involving $0g_{9/2}$ and $0h_{9/2}$ orbitals were included that are required to obtain the Ikeda sum rule. The details for the derivation of the Hamiltonian are described in [9]. In brief, it is obtained with realistic nucleon–nucleon interaction renormalized to the jj77 model space, and with single-particle energies adjusted to reproduce the experimental values observed in ^{131}Sn and ^{133}Sb. This is typical of all shell-model calculations. If single-particle energies are not available from experiment one must rely on those obtained from best Skyrme Hartree–Fock or RMF model extrapolations.

In this work the shell-model calculations for the GT response of ^{132}Sn are performed. Two truncations were used. The simplest called TDA has a closed-shell configuration for ^{131}Sn in the jj55 model space with the addition of two one-particle one-hole final-state configurations, $0g^{(-1)}_{9/2} - 0g^{(1)}_{7/2}$ and $0h^{(-1)}_{11/2} - 0h^{(1)}_{9/2}$. The GT distribution for this is very similar to that obtained with QRPA. For second called TDA + (1p–1h), these TDA configurations were coupled to 1p–1h "vibrations" of the ^{132}Sn core that are obtained within the jj77 model space.

3. Gamow–Teller strength in doubly-magic nuclei

In Fig. 1, we show the results for the GTR in ^{208}Pb obtained within the QRPA, RRPA and RTBA, compared to data of Ref. [20]. The non-relativistic QRPA results are folded by the Lorentz distribution with one MeV width which is close to the energy resolution of the experiment. The parameter $g_{ph} = 1.15$ is adjusted to reproduce the GTR centroid. The QRPA model space, including pn-configurations up to 45 MeV, accommodates the exact Ikeda sum rule while 3% of the total $B(GT_-)$ is beyond the considered 25 MeV energy interval and the total $B(GT_+)$ is equal to 0.21. Without introducing quenching factors in front of the calculated strength

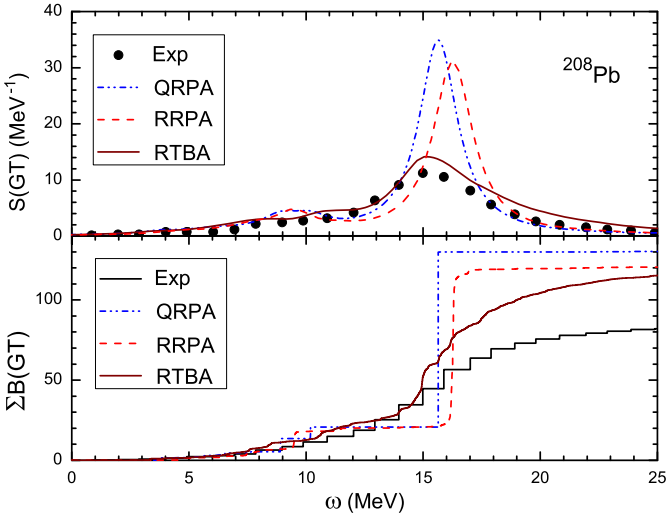

Fig. 1. The theoretical and experimental Gamow–Teller strength distributions in ^{208}Pb (upper panel) and their cumulative sums (lower panel).

function the experimentally observed total strength [20] is by factor 0.62 smaller than that obtained in the QRPA.

The GTR within the relativistic approaches RRPA and RTBA described in Section 2.1 has been calculated using the smearing parameter $\Delta = 1$ MeV. The RRPA calculations, neglecting the last two terms of Eq. (2), produce a strength distribution which is very similar to the non-relativistic QRPA calculations with the major peak at 16.5 MeV and a low-energy peak structure around 10 MeV. The exact Ikeda sum rule is accommodated within the model space of pn-configurations between −1800 MeV and 100 MeV, so that 8% of the $B(GT_-)$ is at large negative energies because of the transitions to the Dirac sea [12]. While both QRPA and RRPA do not account for spreading effects, within RTBA the GTR acquires the spreading width because of the coupling between the ph and ph⊗phonon configurations, so that the additional 5% of the sum rule goes above the considered energy region, while the total $B(GT_+)$ is equal to 0.34. Comparison to data shows that the spreading effects which are taken into account in the RTBA are reproduced very well.

A more detailed analysis of the non-relativistic and relativistic calculations for the GTR in ^{208}Pb has been presented in Fig. 2(a) for both the overall GTR structure (right panels) and the low-lying part (left panels). Compared to Fig. 1, we have reduced the smearing parameter Δ to 200 keV, to see more detailed features of the GTR. Besides this, in Fig. 2 we show the calculated spectra relative to the ground states of daughter nuclei. Since in the present version of the QRPA the effective interaction is not related to any self-consistent mean field, the ground state energies are not defined in this model. However, the single-particle energies entering the QRPA equations are adjusted to data, therefore, for the QRPA we find consistent to use the experimental Q_β values. In contrast, for the self-consistent RRPA and RTBA, in which the effective interaction is the exact second variational derivative of the covariant energy density functional with respect to the density matrix, we use the following formula: $Q_\beta = M(Z,N) - M(Z+1,N-1)$. Here $M(Z,N)$ and $M(Z+1,N-1)$ are the masses of the mother and the daughter nuclei, respectively, calculated in the relativistic mean field by the minimization of the CEDF. Thus, for ^{208}Pb the main GTR peak appears in the RRPA at about 1.5 MeV higher than in the QRPA. When the coupling to the ph⊗phonon configurations is included by the RTBA, the major GTR peak shifts down by the same 1.5 MeV, however, the centroid remains at the same energy as in RRPA. For the low-lying part of the strength distribution, in

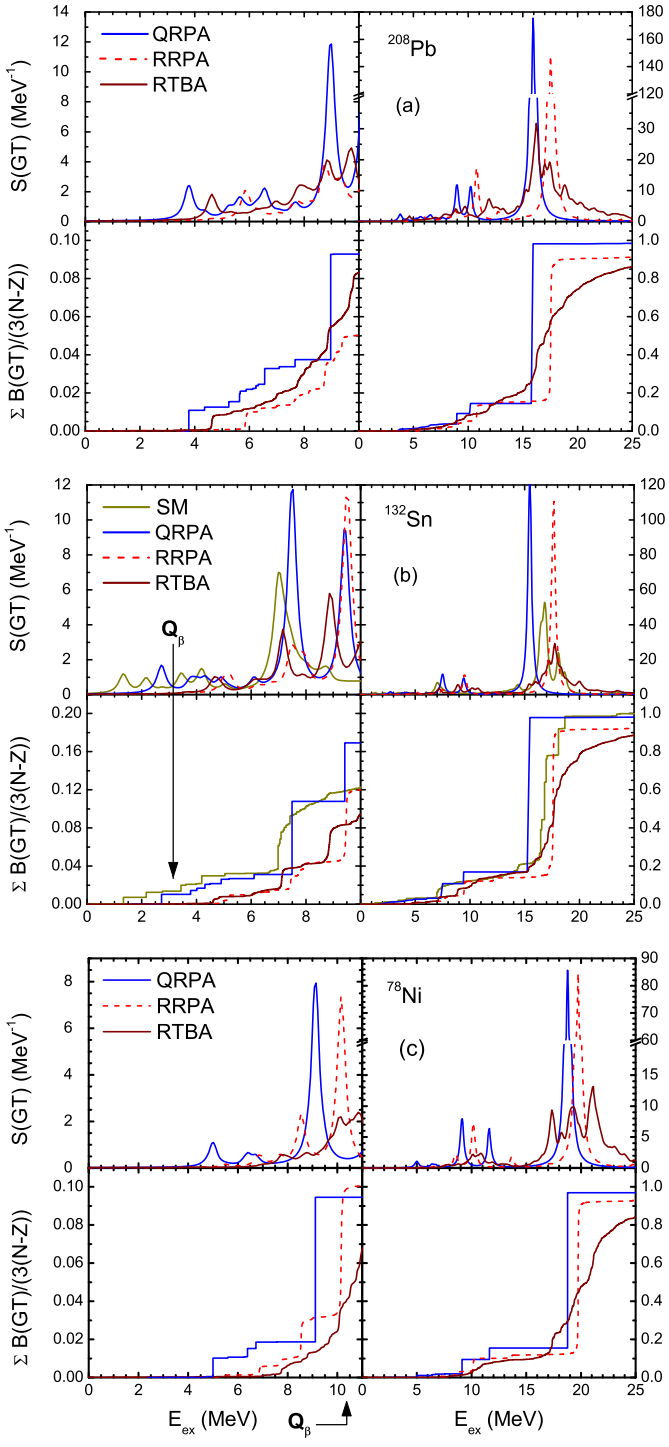

Fig. 2. The Gamow–Teller strength distribution in ^{208}Pb (a) and in neutron-rich ^{132}Sn (b) and ^{78}Ni (c). The SM curves for ^{132}Sn are from the shell-model results for TDA coupled to 1p–1h "vibrations".

particular, for the first excited state, the RTBA calculation shows a much better agreement with the QRPA than the RRPA result. Correlations of the PVC type in the RTBA increase the nucleon effective mass and single-particle level density up to their realistic values [24], which, in turn, causes spreading of the strength to the low-energy region. Single-particle levels used in the QRPA are adjusted to data and, therefore, account for the self-energy part of these correlations implicitly. An additional fine tuning of the g_{ph} and g_{pp} parameters takes into account effectively the phonon-exchange PVC correlations, so that the QRPA built in this way describes successfully gross features of the excitation spectra without explicit treatment of the correlations beyond the one-phonon ones.

The GTR for ^{132}Sn is shown in Fig. 2(b) in the same fashion as for ^{208}Pb. The same parameter sets as for ^{208}Pb are used here within RRPA and RTBA. We have included also results from the shell model calculations for TDA coupled to 1p–1h "vibrations" described in Section 2.3. For the QRPA we used the bare value of $g_{ph} = 1$ without a renormalization, since experimental data on the GT transition strength are not yet available for this nucleus. Here we can see how the QRPA results will compare with the other models without renormalization, because setting $g_{ph} = 1$ is the usual practice for experimentally unknown nuclei. The shell model TDA results (not shown in Fig. 2(b)) are very similar to the QRPA results. The gross structures of the GTR obtained within QRPA and RRPA are very similar except the fact that the overall RRPA strength distribution is shifted upwards by ≈ 2 MeV relative to the QRPA strength. This difference appears when we relate the GTR strength to the ground state of the daughter nucleus, which is done self-consistently in the RRPA and using the experimental Q_β values in QRPA. The inclusion of coupling to the ph⊗phonon configurations by the RTBA leads to a strong fragmentation of the major GTR peak. However, the centroid of the distribution does not shift, and the low-lying strength distribution changes very little.

Within the SM, coupling between the Tamm–Dancoff proton–neutron phonons and particle–hole core vibrations produces strength which is more fragmented than seen in the QRPA and RRPA calculations, but less than in the RTBA calculations, because of the truncation of the SM valence space. The SM strength is also related to the ground state of the daughter nucleus. As the single-particle energies in the SM are adjusted to data and the ground state energies are not defined in this model, it is consistent to use the experimental Q_β values. This practically means that the energy of the first 1^+ state in the SM matches its experimental position. Thus, we see that QRPA overestimates the experimental 1^+_1 energy by 1.5 MeV, but underestimates the centroid predicted by the SM calculation by a similar value. The latter, however, can be changed by tuning the g_{ph} parameter.

Below seven MeV, there is basically the same amount of strength for the SM and QRPA, while in the Q-value window, due to over-predicted 1^+ energy, less strength contributes to β-decay for QRPA. As for the RTBA, while the GTR centroid and width are in a reasonable agreement with the SM calculations, the spreading to the low-energy region is weaker. However, there are at least two mechanisms which are not taken into account in the amplitude $\Phi(\omega)$ of Eq. (5) in the present calculations: coupling to pairing vibrations and the ground state correlations caused by the ph⊗phonon configurations in the response function. These two effects, along with higher-order particle–vibration couplings, can reinforce the spreading to the low-energy region and will be included on the next step of the charge-exchange RTBA development. All the models exhaust the Ikeda sum rule completely within their model spaces, but it can be seen from Fig. 2(b) that 2%, 8% and 12% of the sum rule are beyond the considered energy region in the QRPA, RRPA and RTBA calculations, respectively.

In order to compare the models on a deeper level, we have considered the contributions of the individual neutron–proton transitions to the strength distributions, namely to the main GT peak and to the most pronounced low-lying peak. Table 1 shows these contributions in terms of the reduced matrix elements. For all the models, the matrix elements of the transition densities entering Eq. (11) can be uniformly defined as:

$$X^{1+}_{m,pn} = \langle m||\left[c^\dagger_p c_n\right]^{1^+}||g.s.\rangle, \tag{13}$$

Table 1
Reduced matrix elements for the neutron–proton transitions which contribute mostly to the strength of the major GT peak (GTR) and to the strongest peak at low energy, computed for the considered models. See text for detailed explanations.

m	pn	QRPA		RRPA		RTBA		SM	
		$\langle p\|\|\tau_-\boldsymbol{\sigma}\|\|n\rangle$	$X^{1+}_{m;pn}$	$\langle p\|\|\tau_-\boldsymbol{\sigma}\|\|n\rangle$	$X^{1+}_{m;pn}$	$\langle p\|\|\tau_-\boldsymbol{\sigma}\|\|n\rangle$	$X^{1+}_{m;pn}$	$\langle p\|\|\tau_-\boldsymbol{\sigma}\|\|n\rangle$	$X^{1+}_{m;pn}$
GTR	$\pi h_{9/2} - \nu h_{11/2}$	4.67	0.74	4.54	0.68	4.54	0.37	4.67	0.31
	$\pi g_{7/2} - \nu g_{9/2}$	4.22	0.47	4.10	0.49	4.10	0.32	4.22	0.26
	$\pi h_{11/2} - \nu h_{11/2}$	3.77	0.23	3.60	0.22	3.60	0.12	3.77	0.12
	$\pi d_{3/2} - \nu d_{5/2}$	3.10	0.22	3.01	0.21	3.01	0.11	3.10	0.13
	$\pi g_{7/2} - \nu g_{7/2}$	−2.49	−0.17	−2.32	−0.16	−2.32	−0.08	−2.49	−0.07
Low-energy peak	$\pi g_{7/2} - \nu g_{9/2}$	4.22	0.56	4.10	0.35	4.10	0.06	4.22	0.22
	$\pi d_{3/2} - \nu d_{5/2}$	3.10	−0.49	3.01	−0.62	3.01	−0.14	3.10	
	$\pi h_{11/2} - \nu h_{11/2}$	3.77	−0.33	3.60	−0.15	3.60	−0.15	3.77	−0.27
	$\pi d_{5/2} - \nu d_{5/2}$	2.90	−0.31	2.77	−0.30	2.77	−0.10	2.90	−0.17
	$\pi s_{1/2} - \nu s_{1/2}$	2.45	−0.31	2.36	−0.34	2.36	−0.12	2.45	−0.16
	$\pi h_{9/2} - \nu h_{11/2}$	4.67		4.54	0.21	4.54	0.01	4.67	0.14

where the nucleonic creation and annihilation operators $c^\dagger_p$, c_n are related to the respective basis states. The corresponding backwards going amplitudes $Y^{1+}_{m,pn}$ vanish identically in RRPA, RTBA and SM, and their contributions in QRPA are negligible. As mentioned above, the occupation numbers u_p and v_n are very close to 0 and 1, respectively, in QRPA, and take these values exactly in the other three models. Thus, the products of the reduced matrix elements $\langle p||\tau_-\boldsymbol{\sigma}||n\rangle$ and $X^{1+}_{m,pn}$ displayed in Table 1 contribute to the sum of Eq. (11).

For the GTR one can see that the five largest contributions are represented by the same neutron–proton transitions in all four models and these contributions are coherent. The absolute values of the matrix elements are very close for QRPA and RRPA. Both RTBA and shell model show some reduction of the transition densities, compared to the simpler models, because of the fragmentation effects, but the absolute values of the amplitudes $X^{1+}_{m,pn}$ are close to each other. The matrix elements $\langle p||\tau_-\boldsymbol{\sigma}||n\rangle$ are also very similar in their absolute values for the relativistic and non-relativistic models, and their minor differences reflect the respective differences of the radial wave functions.

The structure of the low-lying GT strength is more sensitive to the differences in single-particle structure and effective interaction and shows more variations from model to model which makes an analysis more difficult. In Table 1 we compare microscopic structure of the strongest low-energy peak below the GTR. The position of the peak depends on the model (see Fig. 2(b)), but, nevertheless, its structure composition reveals considerable similarities. The first 5–6 major contributions come from the same neutron–proton transitions, although their numerical values are different in different models. One can notice, for instance, that the leading component varies from model to model and in all the models except RTBA the leading or the next-to-leading component is out of phase compared to the others which are, in turn, in phase. Thus, the structure of the low-energy peak reveals some destructive interference, in contrast to the GTR peak. In the RTBA the interference is mostly constructive, but the matrix elements $X^{1+}_{m,pn}$ of the leading components have small absolute values since they obey the extended normalization condition (see Eq. (63) of Ref. [44]), which includes sizable phonon coupling contribution. In general, the structure of the low-energy peak in the two models beyond (Q)RPA (RTBA and shell model) shows similarities as well as differences which are expected to be less pronounced if correlations of 3p3h nature will be included. This is the most natural extension of these two models, which is feasible at the current theoretical and computational capacities.

Another doubly magic nucleus of great importance for astrophysics is ^{78}Ni, for which the calculated GTR distributions are displayed in Fig. 2(c). Only three of the considered models: QRPA, RRPA and RTBA are applied to the GTR in this nucleus. Since shell model calculations are based on experimental data about single-particle energies which are not yet known for ^{78}Ni, shell model calculations are not presented. We keep the self-consistent calculation scheme for RRPA and RTBA and use $g_{ph} = 1$ without renormalization for QRPA, because of the absence of experimental data. Like in the previous case, very similar distributions for GTR are obtained within the QRPA and RRPA calculations, except for the positions of the peak structures. They differ by ~ 1 MeV, which is within the range of reasonable tuning for the g_{ph} parameter used in QRPA. The RTBA gives a much richer structure in the region of the main GT peak, and the low-energy fraction is slightly diminished compared to RRPA. The results for the cumulative sums are similar to the previous cases: 8% and 17% of the RRPA and RTBA total GT$_-$ strength, respectively, are beyond the considered 0–25 MeV energy region while only 3% of the total strength is beyond this interval in QRPA. As before, the Ikeda sum rule is exhausted within the full model spaces in all three models.

The nucleus ^{78}Ni is far from the valley of stability and its β-decay Q-value is 10.37 MeV, so that relatively many GT transitions are involved in the β-decay. Within the QRPA the integral strength of these transitions is about one tenth of the total strength, but only the lowest-energy portion contributes to β-decay rate because of the phase space factor. While for RRPA nearly the same amount of strength has been involved, all the strength has been distributed at higher energies. The RTBA spreads the strength more widely, some of the strength is shifted to higher energies, and compared to RRPA, there is a reduction of the decay width. This can be interpreted as the effective quenching of the RRPA strength, and with quenching factors defined in this way, one can obtain an approximate decay width from RRPA or QRPA calculations.

4. Conclusions and outlook

We compare Gamow–Teller response of doubly-magic nuclei computed within the newly developed proton–neutron relativistic time blocking approximation based on the CDFT, QRPA with G-matrix effective interaction and the large-basis shell model. The QRPA and RTBA models are successfully tested, bench marked to experimental data on GTR in ^{208}Pb and applied to predict GTR in neutron-rich doubly-magic ^{78}Ni nuclei. All three models are applied to GTR in ^{132}Sn nucleus allowing, for the first time, a comprehensive comparative study.

Such a comparison turns out to be very constructive in defining strong and weak points of the theory and to determine future directions. We have demonstrated, by the choice of the appropriate physics case of the GTR in ^{132}Sn, that very different theoretical

models can constrain each other. QRPA and SM, based on the realistic interactions, work well together as the SM complements the deficiency of the configuration mixing in QRPA. The SM helps to fix the flexible parameters of the QRPA including the explicitly missed dynamics, that makes the QRPA a useful tool for all nuclei. The RTBA can, to a certain extent, provide information that is missing in QRPA and, in addition, can provide part of the quenching factors that are needed for QRPA and SM. In cases where the RTBA model space includes a sufficiently large amount of configurations and finite momentum transfer is taken into account [45], RTBA has a potential to describe the overall GTR quenching fully microscopically, except the contribution from the delta-isobar which is found to be small [41,42].

Comparison between the RTBA and SM calculations has become possible in this work for the first time. Spreading effects of the high-energy GTR mode in ^{132}Sn are described here within the SM and RTBA on the same level of the configuration complexity, namely, particle–hole coupled to the core vibration and rather similar GT strength distributions are obtained. Thus, SM provides further guidance on inclusion of higher-order correlations into the RTBA that could improve its performance for the low-energy region. In turn, RTBA is an advancement in partly resolving the quenching problem, and, in addition, the relativistic mean field extended by the particle–vibration coupling [25,26] can provide the SM with the single-particle energies for nuclei where these energies are not available from data.

Starting from the presented results, further advancements of the discussed methods are anticipated. Data on the overall GTR distribution and low-lying strength in ^{132}Sn are expected from future measurements of spin–isospin properties of exotic nuclei at the rare isotope beam facilities. Such data will provide decisive arguments to constrain many-body coupling schemes of the RTBA and SM as well as the underlying nuclear effective interactions.

Acknowledgements

We acknowledge support from US-NSF grants PHY-1068217, PHY-0822649 (JINA), PHY-1102511 and PHY-1204486. E.L. acknowledges also the support from NSCL.

References

[1] M. Arnould, S. Goriely, K. Takahashi, Phys. Rep. 450 (2007) 97.
[2] G.F. Bertsch, J. Phys. Conf. Ser. 78 (2007) 012005.
[3] P. Navratil, S. Quaglioni, I. Stetcu, B.R. Barrett, J. Phys. G, Nucl. Part. Phys. 36 (2009) 083101.
[4] L. Coraggio, A. Covello, A. Gargano, N. Itaco, T.T.S. Kuo, Prog. Part. Nucl. Phys. 62 (2009) 135.
[5] Y.F. Niu, G. Coló, M. Brenna, P.F. Bortignon, J. Meng, Phys. Rev. C 85 (2012) 034314.
[6] T. Marketin, E. Litvinova, D. Vretenar, P. Ring, Phys. Lett. B 706 (2012) 477.
[7] B.A. Brown, Prog. Part. Nucl. Phys. 47 (2001) 517.
[8] E. Caurier, G. Martínez-Pinedo, F. Nowacki, A. Poves, A.P. Zuker, Rev. Mod. Phys. 77 (2005) 427.
[9] M. Horoi, B.A. Brown, Phys. Rev. Lett. 110 (2013) 222502.
[10] I.N. Borzov, E.L. Trykov, S.A. Fayans, Sov. J. Nucl. Phys. 52 (1990) 627.
[11] J. Engel, M. Bender, J. Dobaczewski, W. Nazarewicz, R. Surman, Phys. Rev. C 60 (1999) 014302.
[12] N. Paar, T. Nikšić, D. Vretenar, P. Ring, Phys. Rev. C 69 (2004) 054303.
[13] P. Sarriguren, E. Moya de Guerra, A. Escuderos, A.C. Carrizo, Nucl. Phys. A 635 (1998) 55.
[14] J. Suhonen, T. Taigel, A. Faessler, Nucl. Phys. A 486 (1988) 91.
[15] M.S. Yousef, V. Rodin, A. Faessler, F. Simkovic, Phys. Rev. C 79 (2009) 014314.
[16] D.-L. Fang, B.A. Brown, T. Suzuki, Phys. Rev. C 88 (2013) 034304.
[17] D.-L. Fang, B.A. Brown, T. Suzuki, Phys. Rev. C 88 (2013) 024314.
[18] V.A. Kuzmin, V.G. Soloviev, J. Phys. G 10 (1984) 1507.
[19] S. Drożdż, S. Nishizaki, J. Speth, J. Wambach, Phys. Rep. 197 (1990) 1.
[20] T. Wakasa, M. Okamoto, M. Dozono, K. Hatanaka, M. Ichimura, S. Kuroita, Y. Maeda, H. Miyasako, T. Noro, T. Saito, Y. Sakemi, T. Yabe, K. Yako, Phys. Rev. C 85 (2012) 064606.
[21] P. Ring, Prog. Part. Nucl. Phys. 37 (1996) 193.
[22] D. Vretenar, A.V. Afanasjev, G.A. Lalazissis, P. Ring, Phys. Rep. 409 (2005) 101.
[23] P.F. Bortignon, R.A. Broglia, D.R. Bes, R. Liotta, Phys. Rep. 30 (1977) 305.
[24] E. Litvinova, P. Ring, Phys. Rev. C 73 (2006) 044328.
[25] E. Litvinova, A. Afanasjev, Phys. Rev. C 84 (2011) 014305.
[26] E. Litvinova, Phys. Rev. C 85 (2012) 021303(R).
[27] E. Litvinova, P. Ring, V. Tselyaev, Phys. Rev. C 78 (2008) 014312.
[28] E. Litvinova, P. Ring, V. Tselyaev, Phys. Rev. Lett. 105 (2010) 022502.
[29] X. Roca-Maza, X. Vïnas, M. Centelles, P. Ring, P. Schuck, Phys. Rev. C 84 (2011) 054309.
[30] G.A. Lalazissis, J. König, P. Ring, Phys. Rev. C 55 (1997) 540.
[31] P. Ring, Z.-Y. Ma, N. Van Giai, D. Vretenar, A. Wandelt, L.-G. Cao, Nucl. Phys. A 694 (2001) 249.
[32] V.I. Tselyaev, Phys. Rev. C 88 (2013) 054301.
[33] P. Moller, J. Randrup, Nucl. Phys. A 514 (1990) 1.
[34] M. Bender, J. Dobaczewski, J. Engel, W. Nazarewicz, Phys. Rev. C 65 (2002) 054322.
[35] P. Ring, P. Schuck, The Nuclear Many-Body Problem, Springer, Heidelberg, 1980.
[36] B. Alex Brown, Phys. Rev. C 58 (1998) 220.
[37] R. Machleidt, Phys. Rev. C 63 (2001) 024001.
[38] G. Audi, A.H. Wapstra, Nucl. Phys. A 729 (2003) 337.
[39] B.A. Brown, B.H. Wildenthal, Annu. Rev. Nucl. Part. Sci. 38 (1988) 29.
[40] G. Martinez-Pinedo, A. Poves, E. Caurier, A.P. Zuker, Phys. Rev. C 53 (1996) R2602.
[41] A. Arima, K. Schimizu, W. Bentz, H. Hyuga, Adv. Nucl. Phys. 18 (1987) 1.
[42] I.S. Towner, Phys. Rep. 155 (1987) 263.
[43] E. Caurier, F. Nowacki, A. Poves, Phys. Lett. B 711 (2012) 62.
[44] E. Litvinova, P. Ring, V. Tselyaev, Phys. Rev. C 75 (2007) 064308.
[45] T. Marketin, G. Martínez-Pinedo, N. Paar, D. Vretenar, Phys. Rev. C 85 (2012) 054313.